Manipulating light scattering by nanoparticles with magnetoelectric coupling

Tianhua Feng [1,2,*] Shuaifeng Yang,[1] Ning Lai,[1] Weilian Chen,[1] Danping Pan,[1] Wei Zhang,[1,2]
Alexander A. Potapov [1,2] Zixian Liang,[3] and Yi Xu[1]

[1]*Department of Electronic Engineering, College of Information Science and Technology, Jinan University, Guangzhou 510632, China*
[2]*JNU-IREE RAS Joint Laboratory of Information Technology and Fractal Processing of Signals, Jinan University, Guangzhou 510632, China*
[3]*Institute of Microscale Optoelectronics, Shenzhen University, Shenzhen 518060, China*

Light scattering by nanoparticles can be well understood and manipulated in the framework of induced electromagnetic multipoles. Conventionally, the scattering properties of light by nanoparticles are considered to be a result of superposition of the radiation from the induced multipoles due to their orthogonality. Here, we reveal that the interaction between the electric and magnetic dipoles in adjacent nanoparticles can provide an additional route to manipulate light scattering. Specifically, we show that an all-dielectric dimer can support the magnetoelectric coupling effect, in which the electric/magnetic dipole in one nanoparticle can induce an additional magnetic/electric dipole in the other nanoparticle. Such additional electric and magnetic dipoles can suppress or enhance light extinction, which is determined by the phase relationship with respect to the incident field. Furthermore, the magnetoelectric coupling induced dipoles can modify the far-field scattering pattern and even realize unidirectional forward scattering. As a proof-of-principle demonstration, experimental measurements at microwave frequency were performed, and the results are in good agreement with the theoretical ones. Our results may pave the way for manipulating light scattering and novel wave phenomena with magnetoelectric coupling.

I. INTRODUCTION

Light scattering by nanoparticles has been attracting intensive research attention as it plays an important role in various fields related to optics. Scattering light by the surface plasmon resonance, plasmonic nanoparticles can greatly enhance the light-matter interaction by concentrating the light field at subwavelength scale, facilitating the study of displays, lasers, information technology, and exotic wave manipulation, among others [1–5]. Nevertheless, the loss of metallic materials is an inevitable issue for practical applications, especially at visible frequencies. Recently, it was proposed that dielectric nanoparticles not only can address the loss issue but can also provide a powerful means to manipulate light scattering and wave phenomena [6–8].

For both plasmonic and dielectric nanoparticles, the properties of light scattering can be fundamentally understood with the Mie theory [9]. Generally, the nanoparticles can be induced with electric dipoles (EDs), magnetic dipoles (MDs), and even higher-order multipoles as well as their combinations. Consequently, the result of light scattering by a nanoparticle is the superposition of the scattered wave from all the induced multipoles [10–16]. Although the dipoles and higher-order multipoles can be tuned to tailor the light scattering, their interaction, for example, magnetoelectric coupling or bianisotropy of nanoparticles, was exploited recently to enable various exotic electromagnetic wave phenomena

[17–30]. Magnetoelectric coupling describes the fact that the effective ED/MD of nanoparticles can be induced not only by the incident electric/magnetic field but also by the magnetic/electric field [31–33]. As this property was theoretically proposed and experimentally demonstrated at microwave frequencies, scaling it down to the optical spectrum will be of great interest to introduce more degrees of freedom to tailor light-matter interactions [34–39]. More importantly, the geometric symmetry breaking of a single nanoparticle is usually employed in most works to realize the magnetoelectric coupling, but it is a challenge to independently tailor the electric and magnetic multipoles for magnetoelectric coupling because they are closely related via the induced current in an individual nanoparticle. In contrast, if the electric and magnetic multipoles could be induced in different nanoparticles, this limitation may be released. Therefore, it is interesting to ask whether we can achieve magnetoelectric coupling between nanoparticles. In this way, more flexible schemes could be exploited to manipulate light scattering and exotic wave phenomena.

In this work, we propose a route to tailor the magnetoelectric coupling effect with adjacent nanoparticles other than a single one. We theoretically and experimentally demonstrate that the magnetoelectric coupling between nanoparticles can, indeed, be realized with a simple all-dielectric dimer structure [40–44]. In contrast to common cases in which the excitations of both nanoparticles are the same, we introduce a phase difference to the excitation that can benefit the realization of magnetoelectric coupling. This paper is organized as follows. In Sec. II, we employ the coupled electric and

*thfeng@jnu.edu.cn

magnetic dipole (CEMD) method to establish the theoretical model to explain the possibility of enhancing or suppressing light scattering with magnetoelectric coupling. In Sec. III, we specifically study the scattering properties of light by a Si dimer structure. The optical extinction spectra explicitly show the enhancement and suppression effects, in which the magnetoelectric coupling plays an important role. Numerical simulations have also been conducted to verify the theoretical results. In addition, we demonstrate that the magnetoelectric coupling can even be utilized to realize unidirectional forward scattering. In Sec. IV, we present the microwave experiments as a proof-of-principle demonstration, validating the magnetoelectric coupling effect between nanoparticles for a wide frequency range. The conclusion is presented in the last section.

II. THEORETICAL MODELS

Considering an assembly of nanoparticles in the nonmagnetic environment and under the illumination of a plane wave, the total extinction cross section can be evaluated in the dipole approximation as [45]

$$C_{\text{ext}} = \frac{k}{\epsilon_0 \epsilon_r |E_0|^2} \mathbf{Im} \sum_{j=1}^{N} [\mathbf{E}_{\text{loc}}^*(\mathbf{r}^{(j)}) \cdot \mathbf{p}^{(j)} + \mu_0 \mathbf{H}_{\text{loc}}^*(\mathbf{r}^{(j)}) \cdot \mathbf{m}^{(j)}],$$

(1)

in which k is the wave number in the background medium, ϵ_0 and ϵ_r are the permittivity of vacuum and the dielectric constant of the background medium, μ_0 is the permeability of vacuum, E_0 is the amplitude of the incident electric field, $\mathbf{E}_{\text{loc}}(\mathbf{r}^{(j)})$ and $\mathbf{H}_{\text{loc}}(\mathbf{r}^{(j)})$ are the local fields that excite the jth nanoparticle, and $\mathbf{p}^{(j)}$ and $\mathbf{m}^{(j)}$ are the corresponding induced ED and MD moments, respectively. We can observe from Eq. (1) that if the relative phase of the ED or MD moment was less than π with respect to the incident field, its contribution to the total extinction would be positive. The total extinction would consequently be enhanced. However, if its relative phase was larger than π, the corresponding contribution would be negative. In this case, the total extinction would be suppressed. Therefore, the total extinction can be accordingly tuned to be enhanced or even suppressed by tailoring the relative phase of the induced dipole moment. In conventional cases, the relative phase of the induced dipole moment is usually less than π with respect to the incident plane wave for most individual nanoparticles, leading to considerable light extinction. However, when the coupling effect is involved in an assembly of nanoparticles, the local field includes not only the incident wave but also the scattered wave or secondary wave from the adjacent nanoparticles. It is this secondary wave that provides an efficient route to enhance or suppress the total extinction. More importantly, we have found that the secondary wave can originate from the magnetoelectric coupling effect and can exhibit considerable enhancing or suppressing contributions to the total extinction.

In order to study in detail how the magnetoelectric coupling modifies the total extinction, we study an all-dielectric dimer structure consisting of two Si nanoparticles impinged by a plane wave for simplicity. The configuration is schematically shown in Fig. 1. Two nanoparticles locate at the z axis, along which the plane wave is incident. Convention-
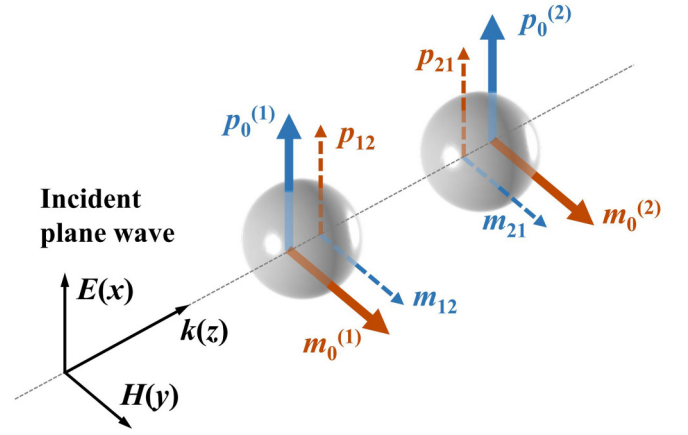

FIG. 1. Schematic showing that an all-dielectric dimer (gray spheres) supports the magnetoelectric coupling under the illumination of a plane wave. $p_0^{(1)}$ and $p_0^{(2)}$ indicate the intrinsic electric dipoles, while $m_0^{(1)}$ and $m_0^{(2)}$ represent the intrinsic magnetic dipoles induced by the incident field in the nanoparticles that encounter the plane wave first and second, respectively. p_{12} and p_{21} are the additional electric dipoles, while m_{12} and m_{21} are the additional magnetic dipoles, which are respectively induced by the magnetic and electric dipoles in the adjacent nanoparticles due to the magnetoelectric coupling effect.

ally, the incident field can induce both EDs and MDs for each nanoparticle in the dipole approximation, as indicated by $\mathbf{p}_0^{(j)}$ and $\mathbf{m}_0^{(j)}$ in Fig. 1. We name them intrinsic dipoles when the two nanoparticles are separated far enough, and then their coupling can be safely neglected. However, when the two nanoparticles approach each other, not only the electric-electric and magnetic-magnetic dipole coupling but also the electric-magnetic coupling should be taken into account. While the former can modify the intrinsic dipole moments, the latter can generate additional dipole moments. We note and show them in Fig. 1 with $\mathbf{p}_{ij}$ and $\mathbf{m}_{ij}$, which show that the ED/MD in the ith nanoparticle is induced by the MD/ED in the jth nanoparticle. This scenario will be explicitly explained in detail in the following context.

For an individual nanoparticle, the local field includes only the incident plane wave. In this case, the induced ED and MD moments can be expressed in the dipole approximation as

$$\mathbf{p}_0^{(j)} = \epsilon_0 \alpha_e^{(j)} \mathbf{E}_0(\mathbf{r}^{(j)}),$$

(2)

$$\mathbf{m}_0^{(j)} = \alpha_m^{(j)} \mathbf{H}_0(\mathbf{r}^{(j)}),$$

(3)

where $\alpha_{e,m}^{(j)}$ is the electric or magnetic polarizability and $\mathbf{E}_0(\mathbf{r}^{(j)})$ and $\mathbf{H}_0(\mathbf{r}^{(j)})$ are the electric and magnetic fields of the incident plane wave at the center of each nanoparticle, respectively. The polarizabilities can be evaluated as $\alpha_e = i6\pi a_1/k^3$ and $\alpha_m = i6\pi b_1/k^3$ with Mie coefficients a_1, b_1 and wave number k, respectively. While the induced dipole moments can be excited by the incident plane wave for an individual nanoparticle, they can also be excited by the secondary field from the adjacent nanoparticle in a dimer. In order to account for the coupling effect between the two nanoparticles, we employ the CEMD method, which can provide a clear physical picture for the coupling of ED and MD moments

[46,47]. Consequently, the induced dipole moments in each nanoparticle can be expressed as

$$\mathbf{p}^{(j)} = \alpha_e^{(j)}[\epsilon_0 \mathbf{E}_0(\mathbf{r}^{(j)})$$
$$+ k^2 \overset{\leftrightarrow}{\mathbf{G}}_{\mathbf{pp}} \cdot \mathbf{p}^{(j')} + ik^2 \epsilon_0 Z_0 \overset{\leftrightarrow}{\mathbf{G}}_{\mathbf{pm}} \cdot \mathbf{m}^{(j')}], \quad (4)$$

$$\mathbf{m}^{(j)} = \alpha_m^{(j)}[\mathbf{H}_0(\mathbf{r}^{(j)})$$
$$- ik^2/\epsilon_0 Z_0 \overset{\leftrightarrow}{\mathbf{G}}_{\mathbf{mm}} \cdot \mathbf{m}_{j'} + k^2 \overset{\leftrightarrow}{\mathbf{G}}_{\mathbf{mp}} \cdot \mathbf{p}_{j'},], \quad (5)$$

where $j, j' = 1, 2$, with $j \neq j'$, Z_0 is the wave impedance of vacuum, and $\overset{\leftrightarrow}{\mathbf{G}}_{\mathbf{pp,mp}}$ and $\overset{\leftrightarrow}{\mathbf{G}}_{\mathbf{mm,pm}}$ are the electric and magnetic dyadic Green's functions, respectively. The second terms on the right-hand sides of Eqs. (4) and (5) are responsible for the electric-electric and magnetic-magnetic coupling effects, respectively. The third terms account for the magnetoelectric coupling effect between nanoparticles. In a specific case in which the two nanoparticles are located at $(0, 0, -d/2)$ and $(0, 0, d/2)$, together with the plane wave excitation conditions $(E_x, E_y, E_z) = (e^{ikz}, 0, 0)$ and $(H_x, H_y, H_z) = (0, e^{ikz}/Z_0, 0)$, the self-consistent coupled equations in Eqs. (4) and (5) can be simplified as

$$p_x^{(1)} = \epsilon_0 \alpha_e^{(1)} e^{-ik\frac{d}{2}} + \alpha_e^{(1)} k^2 A p_x^{(2)} + i\alpha_e^{(1)} \frac{k^2}{c} B m_y^{(2)}, \quad (6)$$

$$m_y^{(1)} = \frac{\alpha_m^{(1)}}{Z_0} e^{-ik\frac{d}{2}} + \alpha_m^{(1)} ik^2 c B p_x^{(2)} + \alpha_m^{(1)} k^2 A m_y^{(2)}, \quad (7)$$

$$p_x^{(2)} = \epsilon_0 \alpha_e^{(2)} e^{ik\frac{d}{2}} + \alpha_e^{(2)} k^2 A p_x^{(1)} - i\alpha_e^{(2)} \frac{k^2}{c} B m_y^{(1)}, \quad (8)$$

$$m_y^{(2)} = \frac{\alpha_m^{(2)}}{Z_0} e^{ik\frac{d}{2}} - \alpha_m^{(2)} ik^2 c B p_x^{(1)} + \alpha_m^{(2)} k^2 A m_y^{(1)}, \quad (9)$$

where c is the speed of light in vacuum, $A = (1 + i/kd - 1/k^2 d^2)e^{ikd}/4\pi d$, and $B = (i - 1/kd)e^{ikd}/4\pi d$. The subscripts x and y indicate the corresponding components of the induced dipole moments, and all other components are zero under this specific excitation condition.

From the equations shown above, it can be noticed that each dipole moment of the constituent nanoparticle is mediated not only by the electric-electric and magnetic-magnetic couplings but also by the magnetoelectric coupling. For example, it is shown in Eq. (6) that in addition to being induced by the incident plane wave, the electric dipole moment of the first nanoparticle is also induced by the secondary wave from both electric and magnetic dipole moments in the other nanoparticles. In addition, the magnetoelectric coupling term shows an order of magnitude similar to that of the electric-electric coupling term, indicating that it could play an important role in the total extinction. In addition, the phase difference in the excitation represented by the first term on the right-hand side of the equations provides a flexible way to tailor the magnetoelectric coupling, in contrast to the case of identical excitation that is usually studied in most works. By numerically solving the four coupled equations, we can evaluate all the dipole moments of the dimer structure as well as their contributions to the extinction cross section by using Eq. (1). In this way, we can unambiguously study how the magnetoelectric coupling modifies the light extinction.
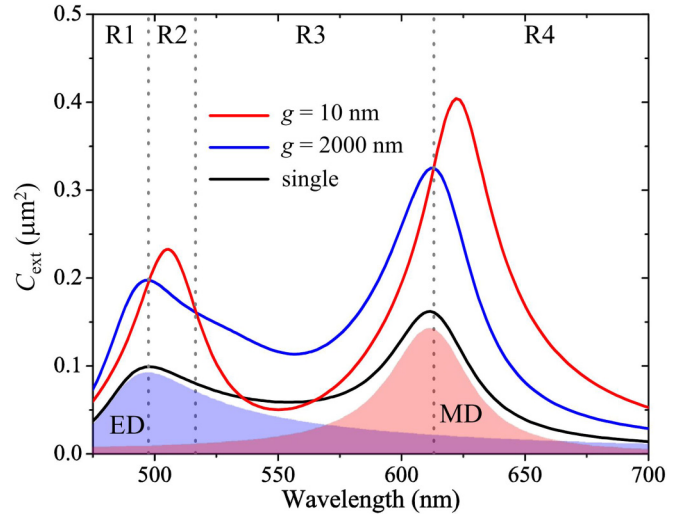

FIG. 2. (a) Total extinction cross section of a Si dimer with a surface-to-surface gap $g = 10$ nm (red line). The results for a dimer with a large gap $g = 2000$ nm (blue line) are also shown as a reference without coupling between nanoparticles. The results for a single nanoparticle (black line) are presented to clarify the nature of the two resonances, which are the ED (blue shading) and MD (red shading) resonances, respectively. Regions R1, R2, R3, and R4, separated by the dashed lines, characterize the spectral regions of the suppressed and enhanced extinction by comparing the cases with different gaps.

III. RESULTS AND DISCUSSION

Without loss of generality, we demonstrate the magnetoelectric coupling effect and the resulting modification of light extinction in the visible spectrum. The radius of both Si nanoparticles is 75 nm, and the surface-to-surface gap between the nanoparticles is $g = 10$ nm. We first calculated the corresponding extinction cross-section spectrum with the dielectric constant of Si fitted from the experimental data [48]. As shown by the red line in Fig. 2, two resonances at about 510 and 620 nm can be identified. To clarify the nature of the resonances, we have calculated and show the extinction spectrum of a single Si nanoparticle. The contributions of ED and MD resonances are presented by the blue and red shading, respectively. It can be found that the resonance at the longer wavelength corresponds to the MD resonance, while that at the shorter wavelength is the ED resonance. In order to explicitly show the coupling effect on the modification of extinction, we have also considered a dimer with a sufficiently large gap of 2000 nm as a reference without the coupling effect, the results of which are also shown in Fig. 2. The extinction is quantitatively about two times that of a single nanoparticle. By comparing the results with different gaps, it can be seen that not only do both resonances shift but also the extinction is obviously changed. Particularly, we can identify four spectral regions according to the suppression or enhancement of extinction, which are indicated by Ri ($i = 1, 2, 3, 4$) in Fig. 2. For example, the extinction at R1 and R3 is suppressed, while that at R2 and R4 is enhanced. Therefore, the coupling between nanoparticles can efficiently modify the extinction spectrum.
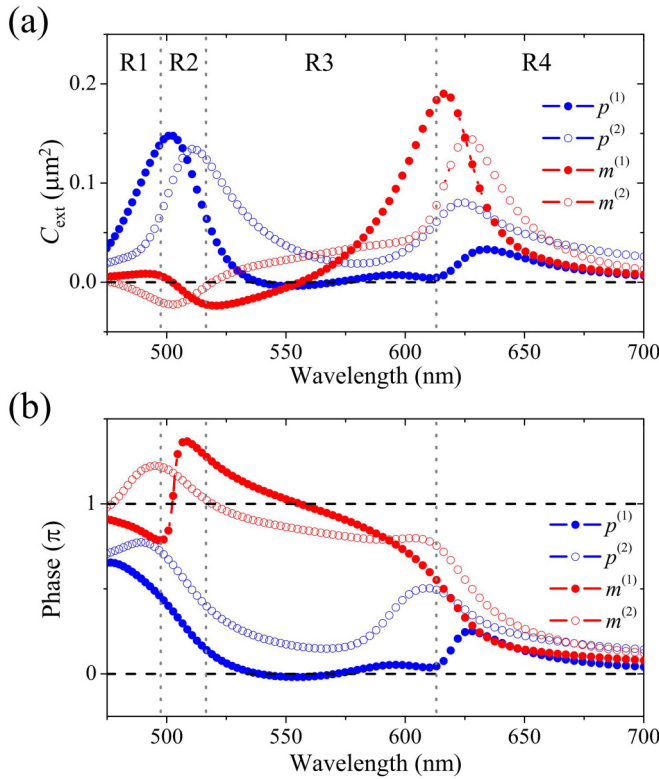
(a)

(b)

FIG. 3. (a) Contributions to the total extinction of ED ($p^{(1)}$ and $p^{(2)}$, blue) and MD ($m^{(1)}$ and $m^{(2)}$, red) in each nanoparticle (solid and open symbols). The horizontal dashed line separates the regions with positive and negative contributions. (b) Corresponding phase relationship of the four induced dipole moments with respect to the incident field. The horizontal dashed lines indicate the phase levels of 0 and π, respectively.

In order to uncover the details on how the coupling affects the extinction, we extract the contributions to the total extinction for all induced dipoles in both nanoparticles with the CEMD model. The results are shown in Fig. 3(a). It can be seen that the contributions of all dipole moments are distinct from that of a single nanoparticle. First, the resonances of all induced dipole moments shift to longer wavelengths. Second, the contribution can be enhanced or suppressed. Third and most importantly, the coupling can greatly modify the spectral line shape at the ED and MD resonances. For instance, besides the intrinsic ED resonance at about 510 nm, an additional ED resonance takes place in both nanoparticles at about the MD resonance, as shown by the blue symbols. This is because the scattered electric field from the intrinsic MD moment in one nanoparticle will polarize the other nanoparticle. Since this MD moment is mainly induced by the incident magnetic field, the additional ED moment can be regarded as the result of the magnetoelectric coupling effect between nanoparticles. The extinction cross section of the additional ED moments around the MD resonances have positive values, and therefore, it can enhance the total extinction. Similar features can be found for the spectrum of the MD around the intrinsic ED resonance, at which the ED resonance in one nanoparticle can induce an additional MD moment in the other. In contrast, the contributions to the total extinction of such additional

MD moments are negative, indicating that they will suppress the extinction. The different signs of the contribution can be understood by examining the relative phases of the induced dipole moments with respect to the incident plane wave. We present the relative phase in Fig. 3(b). It can be seen that the results for MD resonances and additional ED moments are all less than π at about 620 nm. Therefore, they all contribute to the total extinction in a positive way. Nevertheless, the relative phases of the additional MD moments are larger than π at ED resonances of around 500 nm, leading to the suppression of extinction. Consequently, while the electric-electric and magnetic-magnetic couplings modulate the extinction of the intrinsic resonances, the magnetoelectric coupling can contribute considerably to the extinction by inducing additional dipoles in their counterparts. We have also found that the magnetoelectric coupling is robust against the gap distance between the two nanoparticles. Although it becomes weak as the gap is increased, the modification of extinction and additional dipole resonances can still be clearly identified even when the gap is close to the size of the nanoparticles (see Fig. S1 in the Supplemental Material [49]). In addition, the magnetoelectric coupling effect can remain when the incident angle of the light with respect to the center-to-center direction of the dimers is in an acceptable range, thus facilitating the experimental measurements at an optical frequency (see Fig. S2 in the Supplemental Material [49]).

The above theoretical results were obtained from the CEMD model in the point dipole approximation. It is intuitively thought that practical nanoparticles have finite sizes, which should be considered especially when the gap is smaller than the radius. In order to verify the theoretical results, we conducted full-wave simulations with the finite-element method (FEM, COMSOL MULTIPHYSICS 5.2), and the results are presented in Fig. 4. We have simulated the total extinction cross section of a dimer with a gap of 10 nm, and the results are shown in Fig. 4(a). It can be seen that the results show excellent agreement at longer wavelengths, while there are tiny differences at shorter wavelengths. This is because only dipole terms are accounted for in the CEMD model, while all the multipoles are automatically included in the full-wave simulations. We have also examined the contributions to the extinction for all the dipole moments discussed in the CEMD model. We calculated the scattered power of every dipole moment by adopting the multipole decomposition method [50,51]. As shown in Fig. 4(b), the ED and MD resonances can be found for both nanoparticles. More importantly, the magnetoelectric coupling induced additional dipoles at about 510 and 620 nm for MD and ED resonances can also be clearly identified. This means that the magnetoelectric coupling can, indeed, modify the scattering properties of light with the nanoparticles. Therefore, the magnetoelectric coupling effect is robust for a practical structure with a finite size.

While additional dipoles can be induced via magnetoelectric coupling to enhance or suppress the total extinction, they can further provide a platform for tailoring the scattering pattern and even to realize unidirectional scattering by interfering with the intrinsic dipoles [52–54]. To demonstrate this effect, we calculated the forward and backward scattered power spectra of a dimer with $g = 10$ nm via finite-element method (FEM) simulations, which are shown in
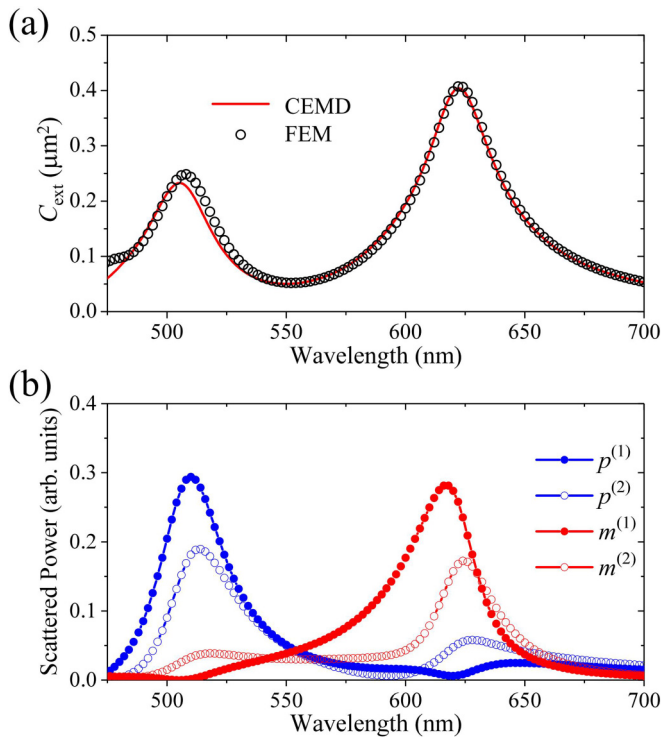
FIG. 4. (a) Total extinction cross-section spectra of a dimer with a gap of 10 nm calculated with the CEMD model (line) and finite-element method (symbols). (b) Scattered power spectra of the four induced dipole moments.
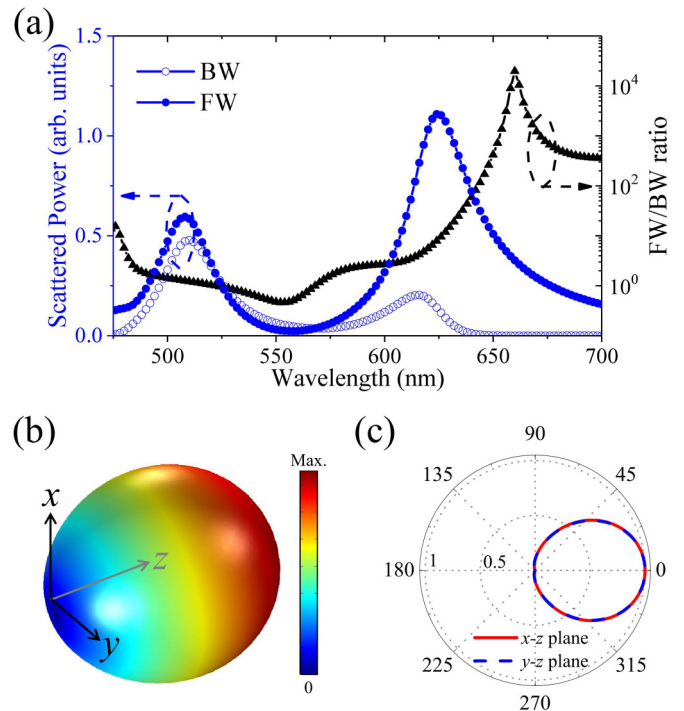

FIG. 5. (a) Forward (blue solid symbols) and backward (blue open symbols) scattering spectra as well as the forward-to-backward scattering ratio (black triangles) spectra of a dimer with $g = 10$ nm. (b) Three-dimensional far-field scattering pattern at a wavelength of 660 nm. (c) Corresponding 2D far-field scattering patterns in the x-z and y-z planes.

Fig. 5(a). It can be noticed that at about the ED and MD resonance, both forward scattering and backward scattering exist. However, away from the MD resonance and at longer wavelengths, the backward scattering decreases rapidly, while the forward one still remains at a considerable level. We have calculated the forward-to-backward scattering ratio and show them in Fig. 5(a). The forward scattering can be larger than the backward one by more than four orders of magnitude, indicating the realization of unidirectional forward scattering. The three-dimensional far-field scattering pattern at a wavelength of 660 nm is shown in Fig. 5(b), and the two-dimensional (2D) patterns in both the x-z and y-z planes are also presented in Fig. 5(c). From these results, we can see that broadband unidirectional scattering can, indeed, be realized with the magnetoelectric coupling effect. Therefore, the magnetoelectric coupling effect can be employed to realize efficient Huygens' sources for on-demand wave-front engineering [55].

IV. EXPERIMENTS AT MICROWAVE FREQUENCIES

Although the magnetoelectric coupling effect and the modified scattering properties are discussed at optical frequencies in the context above, the underlying physics is general, and it can be applied to a wide range of electromagnetic spectra. Here, we experimentally demonstrate a similar conclusion at microwave frequencies. To measure the scattering properties for a dielectric dimer, we built an angle-resolved scattering measurement setup, which is shown in Fig. 6(a). A standard gain horn antenna (HD-58SGAH20N, HengDa Microwave) is connected to a vector network analyzer (VNA, ZNB40, R&S) for exciting microwave at frequencies from 4 to 7.5 GHz. A homemade loop antenna as a probe is also connected to the VNA to measure the magnetic field of the microwave, as shown in Fig. 6(b). The loop antenna is mounted on a rotator so that the magnetic field can be measured in a circular manner around the sample, which is placed on a foam platform. We also placed the absorber around the setup to minimize the unwanted echo signals. The dimer consists of two dielectric disks ($\epsilon_r = 12$, Eccostock HIK), as shown in Fig. 6(b). The diameter and height of each dielectric disk are about 16.5 and 10.5 mm, respectively. The gap between the two disks is about 1 mm. We have calculated the total extinctions of the dimer, as shown in the inset of Fig. 6(c). As a reference, we also present the results without coupling, which can be regarded as the gap being infinitely large and about two times the extinction cross section of a single disk. In the simulations, the incident microwave propagates along the center-to-center direction of the two disks with the magnetic field along the axis of the disks. The ED and MD resonances can be found at about 5 and 6.9 GHz for the case without coupling, while they both shift to lower frequencies for the case with a small gap. Like in the discussion above, the suppression and enhancement of extinction can be found and are robust against the shape of the scatters and working frequency. Experimentally, we measured the forward scattering spectra for both single and dimer structures. To do this, the magnitude of the incident magnetic field without a sample is first measured by recording
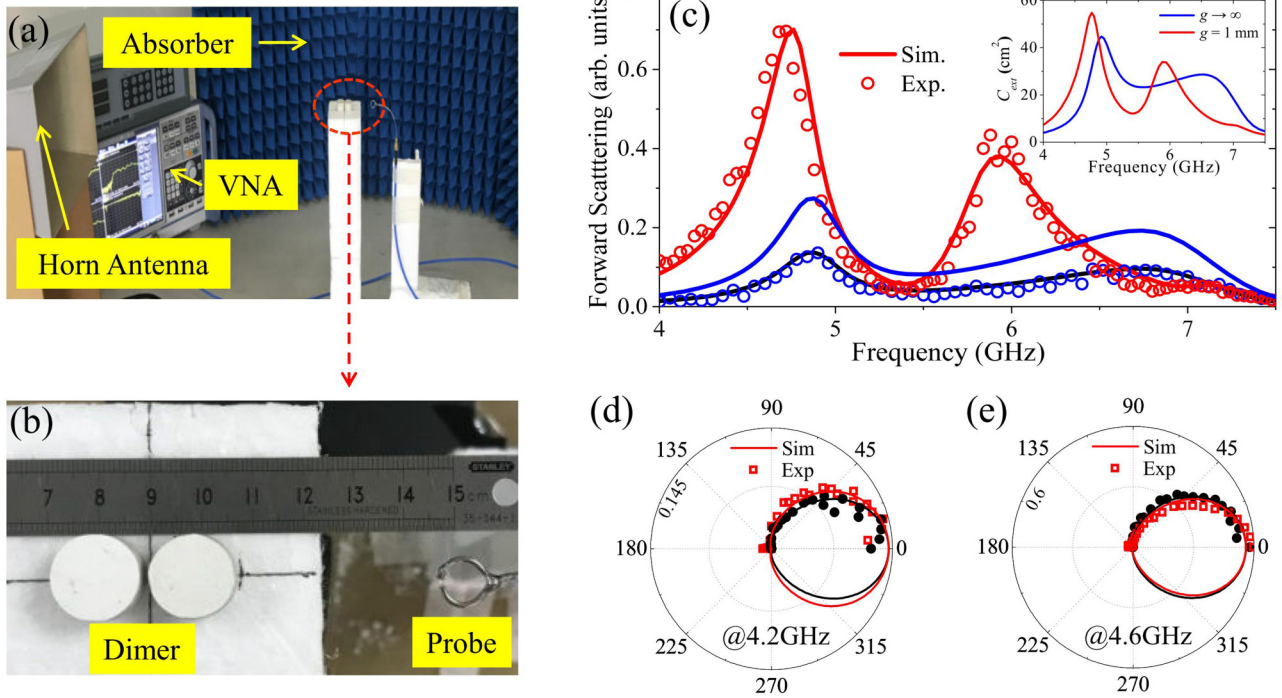
FIG. 6. (a) Experimental setup for measuring the angle-resolved scattering properties at microwave frequencies. (b) Zoomed-in picture of the dimer sample and loop antenna probe. (c) Simulated (line) and measured (circles) forward scattering intensity spectra of a single disk (black) and a dimer (red). The case without coupling (blue line) is evaluated by multiplying the results of a single disk by a factor of 2. Inset: the simulated results of the total extinction cross section for the dimer structures with gaps of 1 mm and infinity. (d) and (e) Two-dimensional angle-resolved normalized scattering intensity patterns at frequencies of 4.2 and 4.6 GHz. Red and black indicate the results in the E and H planes with respect to the horn antenna, respectively. Both simulated (lines) and experimental (symbols) results are shown.

the S parameters between the horn and loop antennas. Then, the total magnetic field is measured in the same way when the samples are involved. Finally, the scattered field is obtained by subtracting the total field with the incident field. Both simulated and measured results are shown in Fig. 6(c). It can be clearly seen that the results are in good agreement, indicating the validity of our theoretical results. In addition, we have also measured the angle-resolved scattering patterns in the E (horizontal) and H (vertical) planes with respect to the horn antenna, which are shown in Figs. 6(d) and 6(e), respectively. It can be seen that the directional scattering can, indeed, be achieved. At frequencies of both 4.2 and 4.6 GHz, the far-field scattering patterns show a strong forward scattering along the $0°$ direction, while the backward scattering along the $180°$ direction is nearly zero, indicating the realization of unidirectional forward scattering in a wide frequency range. For the ease of comparison, we plotted only half of the experimental data at angles from $0°$ to $180°$. Nevertheless, the data for the other half of the angles are similar to those we present here due to the symmetry. The experimental results coincide with the simulation ones in a good manner, validating the theoretical results discussed above.

V. CONCLUSION

In conclusion, we have theoretically and experimentally demonstrated that the magnetoelectric coupling can be achieved in an all-dielectric dimer structure for manipulating light scattering. The results based on the CEMD model show that the total extinction of a dimer structure can be suppressed or enhanced compared with the case of isolated nanoparticles. The underlying physical mechanism whereby the electric/magnetic dipole resonance in one nanoparticle can induce an additional magnetic/electric dipole resonance in the other plays an important role. In addition to the extinction modification, we showed that the magnetoelectric coupling between nanoparticles can benefit the realization of unidirectional forward scattering. Proof-of-principle experiments were conducted at microwave frequency, and the results show good agreement with the theoretical predictions. Our study could facilitate the research into manipulating light scattering and exotic wave-function metamaterials with magnetoelectric coupling.

[1] C. W. Hsu, B. Zhen, W. Qiu, O. Shapira, B. G. DeLacy, J. D. Joannopoulos, and M. Soljačić, Nat. Commun. **5**, 3152 (2014).

[2] M. A. Noginov, G. Zhu, A. M. Belgrave, R. Bakker, V. M. Shalaev, E. E. Narimanov, S. Stout, E. Herz, T. Suteewong, and U. Wiesner, Nature (London) **460**, 1110 (2009).

[3] M. Gu, Q. Zhang, and S. Lamon, Nat. Rev. Mater. **1**, 16070 (2016).

[4] L. Novotny and N. van Hulst, Nat. Photonics **5**, 83 (2011).

[5] N. Yu, P. Genevet, M. A. Kats, F. Aieta, J. Tetienne, F. Capasso, and Z. Gaburro, Science **334**, 333 (2011).

[6] A. I. Kuznetsov, A. E. Miroshnichenko, M. L. Brongersma, Y. S. Kivshar, and B. Luk'yanchuk, Science **354**, aag2472 (2016).

[7] D. Lin, P. Fan, E. Hasman, and M. L. Brongersma, Science **345**, 298 (2014).

[8] I. Staude and J. Schilling, Nat. Photonics **11**, 274 (2017).

[9] C. F. Bohren and D. R. Huffman, *Absorption and Scattering of Light by Small Particles* (Wiley, New York, 1983).

[10] Z. Ruan and S. Fan, Phys. Rev. Lett. **105**, 013901 (2010).

[11] W. Liu and Y. S. Kivshar, Opt. Express **26**, 13085 (2018).

[12] T. Feng, Y. Xu, W. Zhang, and A. E. Miroshnichenko, Phys. Rev. Lett. **118**, 173901 (2017).

[13] Z. Sadrieva, K. Frizyuk, M. Petrov, Y. Kivshar, and A. Bogdanov, Phys. Rev. B **100**, 115303 (2019).

[14] V. E. Babicheva and A. B. Evlyukhin, Phys. Rev. B **99**, 195444 (2019).

[15] T. Feng, A. A. Potapov, Z. Liang, and Y. Xu, Phys. Rev. Appl. **13**, 021002 (2020).

[16] J. Mun, S. So, J. Jang, and J. Rho, ACS Photonics **7**, 1153 (2020).

[17] R. Marques, F. Medina, and R. Rafii-El-Idrissi, Phys. Rev. B **65**, 144440 (2002).

[18] K. Aydin, Z. Li, M. Hudlicka, S. A. Tretyakov, and E. Ozbay, New J. Phys. **9**, 326 (2007).

[19] Z.-G. Dong, S.-Y. Lei, Q. Li, M.-I. Xu, H. Liu, T. Li, F.-M. Wang, and S.-N. Zhu, Phys. Rev. B **75**, 075117 (2007).

[20] C.-W. Qiu, H.-Y. Yao, L.-W. Li, S. Zouhdi, and T.-S. Yeo, Phys. Rev. B **75**, 245214 (2007).

[21] F. Liu, Z. Liang, and J. Li, Phys. Rev. Lett. **111**, 033901 (2013).

[22] C. Kriegler, M. S. Rill, S. Linden, and M. Wegener, IEEE J. Sel. Top. Quantum Electron. **16**, 367 (2010).

[23] E. Plum, X.-X. Liu, V. A. Fedotov, Y. Chen, D. P. Tsai, and N. I. Zheludev, Phys. Rev. Lett. **102**, 113902 (2009).

[24] C. Pfeiffer and A. Grbic, Phys. Rev. Appl. **2**, 044011 (2014).

[25] C. Menzel, C. Helgert, C. Rockstuhl, E.-B. Kley, A. Tünnermann, T. Pertsch, and F. Lederer, Phys. Rev. Lett. **104**, 253902 (2010).

[26] R. Alaee, M. Albooyeh, M. Yazdi, N. Komjani, C. Simovski, F. Lederer, and C. Rockstuhl, Phys. Rev. B **91**, 115119 (2015).

[27] V. S. Asadchy, Y. Ra'di, J. Vehmas, and S. A. Tretyakov, Phys. Rev. Lett. **114**, 095503 (2015).

[28] Y. Ra'di, D. L. Sounas, and A. Alù, Phys. Rev. Lett. **119**, 067404 (2017).

[29] A. Epstein and G. V. Eleftheriades, Phys. Rev. Lett. **117**, 256103 (2016).

[30] G. Guo, T. Feng, and Y. Xu, Opt. Lett. **43**, 4961 (2018).

[31] L. D. Landau and E. M. Lifshitz, *Electrodynamics of Continuous Media* (Pergamon, Oxford, 1960).

[32] A. Serdyukov, I. V. Semchenko, S. A. Treyakov, and A. Sihvola, *Electromagnetics of Bi-anisotropic Materials: Theory and Application* (Gordon and Breach, Amsterdam, 2001).

[33] J. Li, A. Salandrino, and N. Engheta, Nanophotonics **7**, 1069 (2018).

[34] Y. Yang, I. I. Kravchenko, D. P. Briggs, and J. Valentine, Nat. Commun. **5**, 5753 (2014).

[35] M. Albooyeh, R. Alaee, C. Rockstuhl, and C. Simovski, Phys. Rev. B **91**, 195304 (2015).

[36] A. E. Miroshnichenko, A. B. Evlyukhin, Y. S. Kivshar, and B. N. Chichkov, ACS Photonics **2**, 1423 (2015).

[37] R. Alaee, M. Albooyeh, A. Rahimzadegan, M. S. Mirmoosa, Y. S. Kivshar, and C. Rockstuhl, Phys. Rev. B **92**, 245130 (2015).

[38] D. Markovich, K. Baryshnikova, A. Shalin, A. Samusev, A. Krasnok, P. Belov, and P. Ginzburg, Sci. Rep. **6**, 22546 (2016).

[39] M. Albooyeh, V. S. Asadchy, R. Alaee, S. M. Hashemi, M. Yazdi, M. S. Mirmoosa, C. Rockstuhl, C. R. Simovski, and S. A. Tretyakov, Phys. Rev. B **94**, 245428 (2016).

[40] C. Wang, Z. Y. Jia, K. Zhang, Y. Zhou, R. H. Fan, X. Xiong, and R. W. Peng, J. Appl. Phys. **115**, 244312 (2014).

[41] Z.-Y. Jia, J.-N. Li, H.-W. Wu, C. Wang, T.-Y. Chen, R.-W. Peng, and M. Wang, J. Appl. Phys. **119**, 074302 (2016).

[42] Á. I. Barreda, H. Saleh, A. Litman, F. González, J.-M. Geffrin, and F. Moreno, Nat. Commun. **8**, 13910 (2017).

[43] T. Shibanuma, T. Matsui, T. Roschuk, J. Wojcik, P. Mascher, P. Albella, and S. A. Maier, ACS Photonics **4**, 489 (2017).

[44] T. Das and J. A. Schuller, Phys. Rev. B **95**, 201111(R) (2017).

[45] A. B. Evlyukhin, C. Reinhardt, A. Seidel, B. S. Luk'yanchuk, and B. N. Chichkov, Phys. Rev. B **82**, 045404 (2010).

[46] G. W. Mulholland, C. F. Bohren, and K. A. Fuller, Langmuir **10**, 2533 (1994).

[47] P. Albella, M. A. Poyli, M. K. Schmidt, S. A. Maier, F. Moreno, J. José Sáenz, and J. Aizpurua, J. Phys. Chem. C **117**, 13573 (2013).

[48] E. D. Palik, *Handbook of Optical Constants of Solids* (Academic, London, 1998).

[49] See Supplemental Material at http://link.aps.org/supplemental/10.1103/PhysRevB.102.205428 for the gap dependence of magnetoelectric coupling and the dimer-orientation dependence of magnetoelectric coupling.

[50] T. Kaelberer, V. A. Fedotov, N. Papasimakis, D. P. Tsai, and N. I. Zheludev, Science **330**, 1510 (2010).

[51] Y. He, G. Guo, T. Feng, Y. Xu, and A. E. Miroshnichenko, Phys. Rev. B **98**, 161112(R) (2018).

[52] Y. H. Fu, A. I. Kuznetsov, A. E. Miroshnichenko, Y. F. Yu, and B. Luk'yanchuk, Nat. Commun. **4**, 1527 (2013).

[53] D. Pan, T. Feng, W. Zhang, and A. A. Potapov, Opt. Lett. **44**, 2943 (2019).

[54] M. Liu, Y. Xie, T. Feng, and Y. Xu, Opt. Lett. **45**, 968 (2020).

[55] C. Pfeiffer and A. Grbic, Phys. Rev. Lett. **110**, 197401 (2013).